Cycling Characteristics of Lithium Powder Polymer Batteries Assembled with Composite Gel Polymer Electrolytes and Lithium Powder Anode

Yoon-Sung Lee, Jae Ha Lee, Ji-Ae Choi, Woo Young Yoon, and Dong-Won Kim**

Novel composite gel polymer electrolytes exhibiting high ionic conductivity and good mechanical stability are prepared, and their electrochemical properties are characterized. As lithium ion sources of a single ion conductor, the core-shell structured $SiO_2(Li^+)$ nanoparticles with uniform spherical shape are synthesized and used as functional fillers in the composite gel polymer electrolytes. By using the composite gel polymer electrolytes, the lithium powder polymer batteries composed of a lithium powder anode and a layered lithium vanadate (LiV_3O_8) cathode are assembled and their cycling performance is evaluated. The resulting lithium powder polymer batteries deliver a high discharge capacity of 264 mAh g^{-1} at room temperature and exhibit good capacity retention even at high current rates. The morphological analysis of the lithium powder anode reveals that the dendrite growth during cycling can be effectively suppressed by using the composite gel polymer electrolytes.

1. Introduction

Rechargeable lithium batteries using lithium metal as an anode material are attractive candidates for high energy density power sources in portable electronic devices, electric vehicles and energy storage systems, because the lithium metal offers the highest specific capacity (~3862 mAh g^{-1}) for an active negative electrode material.[1] However, the use of lithium metal anode has been limited by the occurrence of dendrite growth during repeated charge and discharge cycles. The formation and growth of lithium dendrites give rise to safety problems and gradual degradation of cycling efficiency.[2–4] Therefore, the control of dendritic growth is important for developing the lithium metal batteries with enhanced safety and good capacity retention. In previous studies, the compacted lithium powder instead of lithium foil was suggested as a new anode material to prevent dendritic growth.[5–8] The cycling efficiency of lithium powder electrode was higher than that of lithium foil electrode.[5] The control of solid electrolyte interface (SEI) on lithium powder electrode demonstrated that the electrochemical properties and safety of lithium powder anodes could be improved.[6–8] The use of safe liquid electrolytes is another issue that must be considered in the successful development of lithium metal batteries. Highly flammable organic solvents in common liquid electrolytes may cause fires or explosions due to short circuits or local overheating. The quest for safer and more reliable electrolyte systems is therefore urgent, and polymer electrolytes are promising candidates in this regard.[1,9–13] After the first suggestion that poly(ethylene oxide) (PEO) could be used as a polymer-based solid electrolyte,[9] solid polymer electrolytes have been considered ideal alternatives to liquid electrolytes. However, their low ionic conductivities, ranging from 10^{-8} to 10^{-5} S cm^{-1}, preclude their practical applications for use in lithium batteries at ambient temperatures. Accordingly, most relevant research has focused on the preparation and characterization of gel polymer electrolytes that exhibit higher ionic conductivities at room temperature.[14,15] Such gel polymer electrolytes encapsulate a large amount of liquid electrolyte in matrix polymer, and their ionic conductivities usually exceed 10^{-3} S cm^{-1} at room temperature, which is necessary for battery applications. Gel polymer electrolytes are also more flexible than conventional inorganic glass or ceramic electrolytes, which enables them to conform to the volume change of both electrodes (anode and cathode) during charge-discharge cycling. Polyacrylonitrile (PAN), poly(vinylidene fluoride) (PVdF), poly(vinylidene fluoride-*co*-hexafluoropropylene) (P(VdF-*co*-HFP)) and poly(methyl methacrylate) (PMMA) are the host polymers most commonly used for preparing gel polymer electrolytes.[14–20] However, the host polymers lose mechanical strength when plasticized by organic solvents. Most efforts to increase ionic conductivity by incorporating larger amounts of liquid electrolyte are detrimental to mechanical properties and also cause poor compatibility with lithium electrodes. The high reactivity of lithium metal towards organic solvents negatively affects the cycle life and safety of lithium metal batteries. Accordingly, to obtain the gel polymer electrolytes with improved electrical and mechanical properties, ceramic fillers such as SiO_2, Al_2O_3, TiO_2 and $BaTiO_3$ have been incorporated

Y.-S. Lee, J.-A. Choi, Prof. D.-W. Kim,
Department of Chemical Engineering
Hanyang University
Seoul 133-791, Korea
E-mail: dongwonkim@hanyang.ac.kr
J. H. Lee, Prof. W. Y. Yoon
Department of Materials Science and Engineering
Korea University
Seoul 136-701, Korea
E-mail: wyyoon@korea.ac.kr

DOI: 10.1002/adfm.201200692

into host polymers.[12,21–30] The addition of ceramic fillers improves ionic conductivity of polymer electrolytes and interfacial properties at the lithium electrode, which are important for practical applications in lithium metal batteries. In these composite gel polymer electrolytes, the ceramic particles promote electrochemical properties of the polymer electrolytes, but only by physical actions without directly contributing to the lithium ion transport process. It has been reported that the ceramic filler particles could also act as a source of charge carriers by facilitating suitable surface modifications of particles.[31–33] However, it was difficult to control the morphologies of the resultant ceramic particles containing lithium ions. Thus, it is of great interest to synthesize and introduce nano-sized inorganic materials containing dissociative lithium ions, which are based on a core-shell structure with unique advantages in terms of controlling the final morphology. Layered lithium vanadate (LiV_3O_8) has been considered an attractive electroactive material for use as a cathode in lithium metal batteries.[34–40] Based on theoretical calculations, the lithium vanadate can deliver a high specific capacity (approximately 280 mAh g^{-1} for $3Li^+$ insertion/deinsertion) that is nearly double that of $LiCoO_2$. Additionally, the lithium vanadate works in a potential range in which no side reactions due to electrolyte oxidation are expected.

In this study, we prepared the composite gel polymer electrolytes based on P(VdF-*co*-HFP) and core-shell structured SiO_2 nanoparticles containing lithium ions. The SiO_2 particles have unique core-shell morphology with a thin layer of poly(lithium 4-styrene sulfonate) surrounding a nano-sized SiO_2 core particle. The composite gel polymer electrolyte prepared with core-shell structured SiO_2 particles exhibited high ionic conductivity and good mechanical strength to prepare thin films (~40 μm). Using these gel polymer electrolytes, we assembled lithium powder polymer batteries composed of a lithium powder anode and a LiV_3O_8 cathode. The cycling performances of the batteries were evaluated and compared to those of batteries assembled with liquid electrolyte or lithium foil anode. Our results confirm the superior performance of lithium powder polymer batteries using a core-shell SiO_2-based composite polymer electrolyte and lithium powder anode.

2. Results and Discussion

2.1. Characterization of Core-Shell Structured $SiO_2(Li^+)$ Particles

Figure 1 shows the SEM images of silica core particles obtained after the first step shown in Figure S1. All particles have very uniform spherical shapes with average diameters of approximately 230 to 640 nm. The particle size of the silica cores could

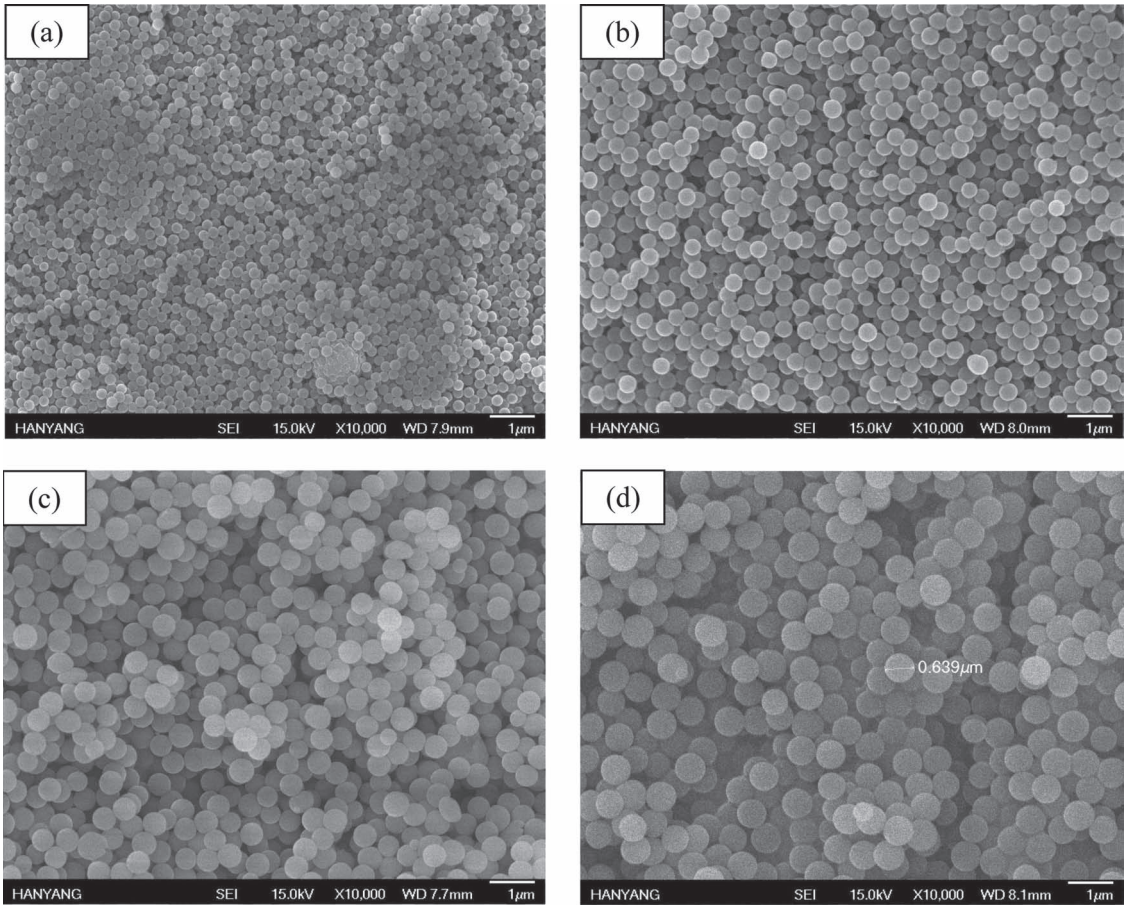

Figure 1. SEM images of SiO_2 core particles with different particle size. In synthesizing the SiO_2 core particles, the concentrations of VTMS were (a) 0.10, (b) 0.15, (c) 0.25 and (d) 0.40 M, respectively.

be controlled by adjusting concentrations of vinyltrimetoxylsilane (VTMS) from 0.10 to 0.40 M in the presence of NH_4OH. FT-IR measurements were performed to confirm the chemical structure of the silica core particles. Symmetric stretching vibrations of the siloxane (Si-O-Si) group appeared at 766 cm^{-1}, while asymmetric stretching vibrations of siloxane were observed between 1200 and 1000 cm^{-1}. The spectrum also revealed two sharp peaks at 1603 and 1410 cm^{-1}, which are characteristic of the C=C double bond introduced by the VTMS molecules,[41–44] indicating that the silica core particles contain vinyl groups. These reactive vinyl groups permit the growth of silica particles by radical polymerization with 4-styrenesulfonic acid sodium salt during the second step to produce core-shell structured silica particles. Among the silica core particles obtained at the first step, the particles with a diameter of 400 nm were chosen as the base material for synthesizing core-shell structured SiO_2 particles at the second step.

Core-shell structured SiO_2 nanoparticles were synthesized by radical copolymerization of cored-silica nanoparticles and 4-styrenesulfonic acid sodium salt, as depicted in Figure S1. **Figure 2** shows the TEM image and EDXS profile of a core-shell silica particle containing poly(sodium 4-styrenesulfonte) (PSS) in the shell. The particle has a very uniform core-shell morphology with a 200 nm-thick shell layer of PSS (in gray) surrounding a SiO_2 core particle (in black) (Figure 2(a)). The core diameter was estimated to be about 400 nm. The EDXS profile in the direction of diameter of the core-shell SiO_2 particle (Figure 2(b)) reveals that the silicon atoms are positioned at the particle core (~400 nm), while sulfur and sodium atoms arising from the PSS appear in the shell (~200 nm). In the shell layer, the atomic ratio of sulfur and sodium was estimated to be about 1.0. These findings are well consistent with the TEM image shown in Figure 2(a), confirming that the SiO_2 particles were encapsulated by PSS with a uniform thickness and that spherical core-shell structured SiO_2 particles were successfully synthesized. The shell layer thickness was controlled by varying the concentration of 4-styrenesulfonic acid sodium salt monomer and the reaction time at the second step in Figure S1. Using these core-shell structured $SiO_2(Na^+)$ particles, we replaced the sodium ions in the shells of the core-shell structured SiO_2 particles with lithium ions. The XPS spectrum of the core-shell structured SiO_2 particles shown in Figure S2 revealed a 57.4 eV characteristic peak corresponding to lithium,[45] confirming that the $SiO_2(Na^+)$ particles converted to $SiO_2(Li^+)$ particles.

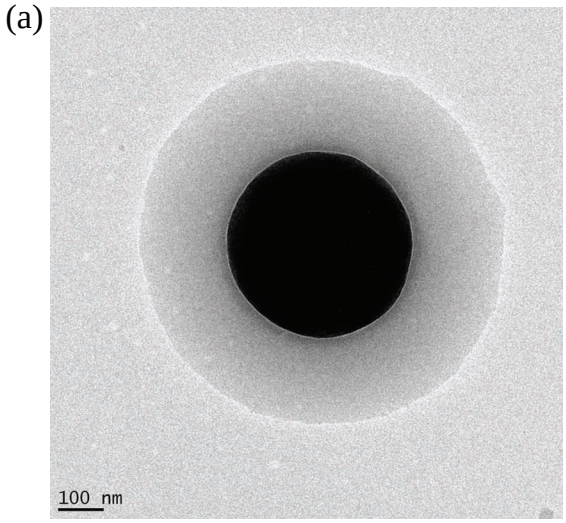

(a) TEM image of core-shell structured SiO_2 particle

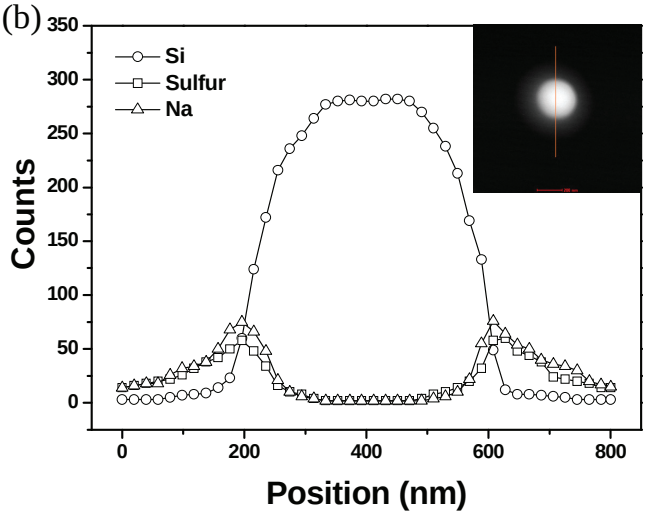

Figure 2. (a) TEM image and (b) EDXS profile of core-shell structured SiO_2 particle in the direction of diameter.

2.2. Composite Gel Polymer Electrolytes Containing $SiO_2(Li^+)$ Particles

Hybrid composite polymer membranes were prepared from P(VdF-*co*-HFP) and core-shell structured $SiO_2(Li^+)$ powders. The addition of $SiO_2(Li^+)$ nanoparticles provided sufficient mechanical integrity to process a free-standing film with a thickness of 40 μm, as shown in Figure S3, and thereby eliminated the need for a cross-linking step. As the content of core-shell silica particle increased, the membrane turned to white opaque film, as illustrated in the figure. EDXS mapping images of the surface of the hybrid composite polymer membrane containing 20 wt.% $SiO_2(Li^+)$ particles are shown in **Figure 3**. The EDXS mapping images illustrate the homogeneous distributions of chosen elements (fluorine, silicone, sulfur) across the image, which suggests that the core-shell structured $SiO_2(Li^+)$ particles are homogeneously distributed in the composite membrane without agglomeration.

A composite gel polymer electrolyte was obtained by soaking the hybrid composite polymer membrane in liquid electrolyte. The electrolyte solution was well encapsulated in the composite gel polymer electrolyte by physical gelation. **Figure 4** is a schematic representation of lithium-ion conduction in the composite gel polymer electrolyte containing core-shell $SiO_2(Li^+)$ particles as a filler. As illustrated in the figure, the lithium ions can dissociate from the core-shell structured $SiO_2(Li^+)$ powders, thus acting as charge carriers. In addition, the incorporation of $SiO_2(Li^+)$ powders resulted in a filler network providing

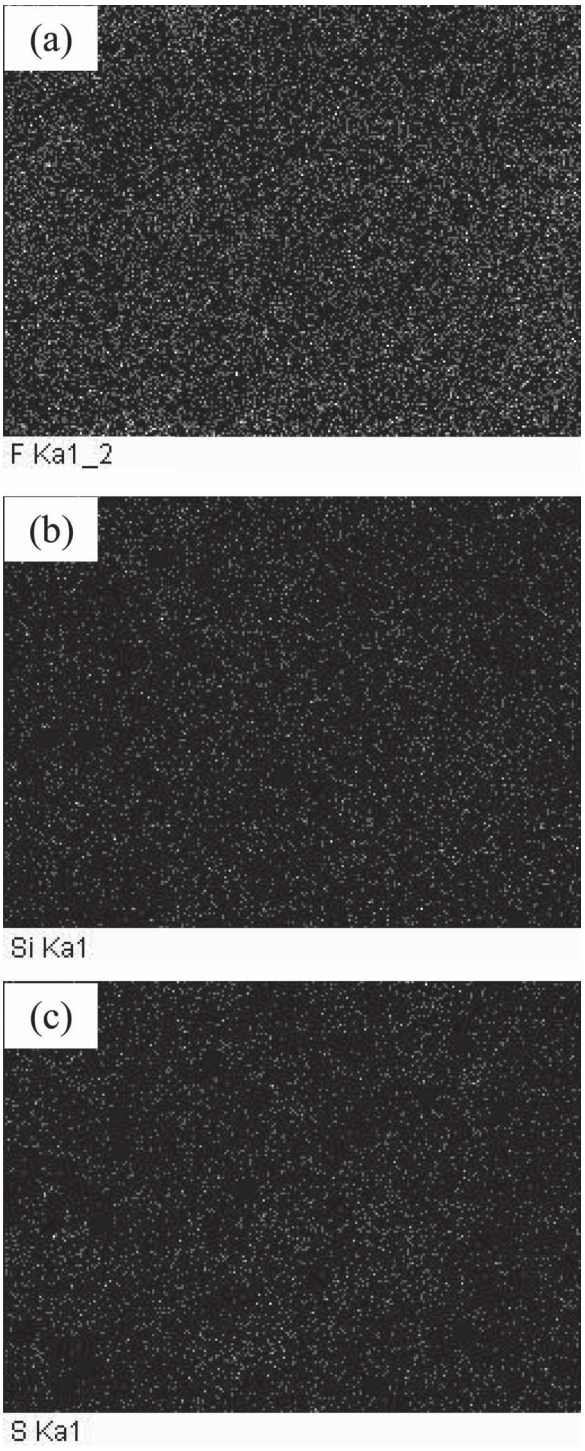

Figure 3. EDXS mapping images of (a) fluorine, (b) silicone and (c) sulfur in the composite polymer membrane containing 20 wt.% core-shell structured $SiO_2(Li^+)$ powders.

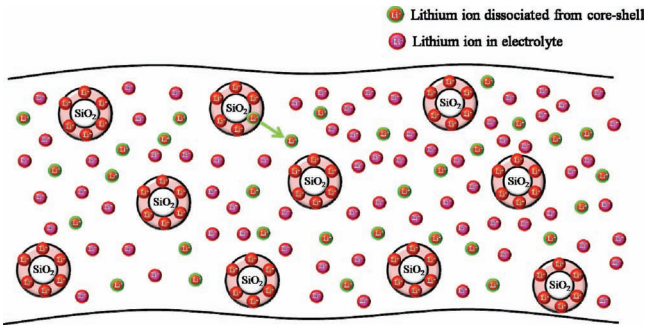

Figure 4. Schematic representation of lithium-ion conduction in the composite gel polymer electrolyte containing core-shell structured $SiO_2(Li^+)$ particles.

mechanical integrity to the gel polymer electrolyte and the consequent formation of free-standing films. **Figure 5** shows the evolution of the ionic conductivity and lithium transport of the composite gel polymer electrolyte as a function of the core-shell structured $SiO_2(Li^+)$ particle content. The ionic conductivity increases with increasing $SiO_2(Li^+)$ particles, up to a maximum at 20 wt.%. The increase in ionic conductivity promoted by the $SiO_2(Li^+)$ particles is associated with the enhancement of electrolyte uptake, as well as the increase in mobile lithium ions dissociating out of the shell of the $SiO_2(Li^+)$ particles. The amount of electrolyte solution absorbed after soaking the membrane in the liquid electrolyte increased with the $SiO_2(Li^+)$ particle content, as shown in Figure S4, which resulted in an increase in ionic conductivity. This is due to the fact that the hydrophilic poly(lithium 4-styrenesulfonte) (PLS) in the shell of core-shell structured $SiO_2(Li^+)$ particle has a high affinity for the electrolyte solution. Moreover, it is confirmed that the lithium transport number increases with increasing content of $SiO_2(Li^+)$ particles in the composite gel polymer electrolytes. It gradually increases from 0.35 to 0.48 upon the addition of $SiO_2(Li^+)$ particles (30 wt.%). The $SiO_2(Li^+)$ particles are intrinsic single ion conductors, since the sulfonate anions ($-SO_3^-$) are anchored to pendant group on the polymer around silica core. Thus it is plausible that the lithium ions dissociated from the $SiO_2(Li^+)$ particles contribute to the ionic conductivity, resulting in an

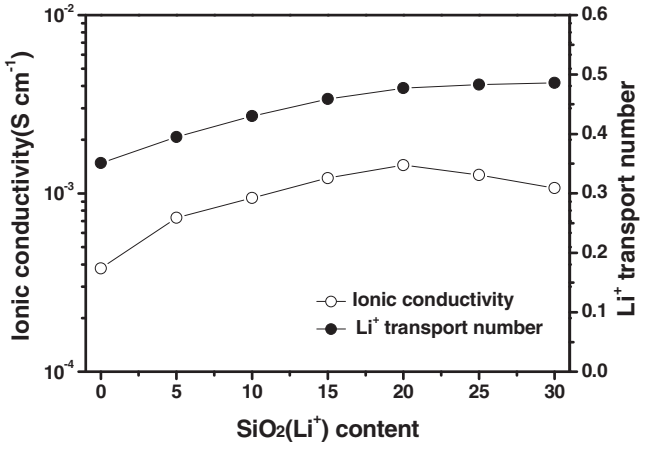

Figure 5. Ionic conductivities and Li^+ transport number of composite gel polymer electrolytes as a function of core-shell structured $SiO_2(Li^+)$ particle content.

increase in the lithium transport number. The generation of a free volume at the interface of the dispersed $SiO_2(Li^+)$ nanoparticles may also contribute to the improved ionic conductivity, as previously reported in other composite polymer electrolyte systems.[25,46] The decrease in ionic conductivity beyond 20 wt.% $SiO_2(Li^+)$ may be attributed to the blocking effect of the charge carrier transport, since the core of the $SiO_2(Li^+)$ powder is an insulator by nature. As a result, the connectivity of the ion conducting phase becomes more tortuous at high $SiO_2(Li^+)$ particle content. Therefore, the addition of 20 wt.% $SiO_2(Li^+)$ powder yielded the most desirable environment for ionic transport in the composite gel polymer electrolyte in this study. The ionic conductivity of the composite gel polymer electrolyte prepared with 20 wt.% $SiO_2(Li^+)$ powders is 1.4×10^{-3} S cm^{-1} at room temperature.

2.3. Cycling Characteristics of Lithium Powder Polymer Batteries

Composite gel polymer electrolytes were used to assemble lithium powder polymer batteries consisting of a lithium powder anode and a LiV_3O_8 cathode. The typical morphology of a lithium powder electrode is shown in Figure S5. The lithium powders are spherical in shape and particle diameters range from 3 to 12 μm. Porous characteristics of the lithium powder electrode could be clearly observed. The surface area of the lithium powder electrode was estimated to be 16 fold higher than that of a lithium foil electrode, according to the current ratio of lithium powder to lithium foil based on linear sweep voltammetry.[47] The larger reactive surface area may lower the effective current density on the electrode surface, which suppresses dendrite formation during cycling of the cells. The SEM image of the LiV_3O_8 powder used in this study is shown in **Figure 6**(a). The morphology of the LiV_3O_8 powder is characterized by lath-like structures with sharp edges. The powders exhibit heterogeneous particle size distribution. Figure 6(b) shows a SEM image of the cathode prepared with LiV_3O_8 powder, carboxymethyl cellulose (CMC) binder and conducting agent. Ketchen blacks as the conductive material are homogeneously dispersed with active LiV_3O_8 powders in the electrode.

The assembled batteries were cycled in the voltage range of 2.0–3.6 V at a constant current rate of 0.2 C. **Figure 7** shows the typical voltage profiles of the 1st, 10th, 20th, 30th and 50th charge-discharge cycles of the lithium powder polymer battery assembled with the composite gel polymer electrolyte containing 20 wt.% $SiO_2(Li^+)$ particles. The battery exhibited discharge plateaus near 2.8 and 2.6 V, delivering an initial discharge capacity of 264 mAh g^{-1} based on the LiV_3O_8 active material in the cathode. The 2.8 V discharge plateau corresponds to the single-phase insertion process and the 2.6 V plateau is ascribed to the two-phase transformation between $Li_{1+x}V_3O_8$ ($1 \le x \le 2$) and $Li_4V_3O_8$, as previously reported.[39,48] The voltage drops in passing from charge to discharge are observed to be small, which suggests that the battery has very low internal cell resistance and is capable of delivering high capacity. The discharge capacity declined to 242 mAh g^{-1} at the 50th cycle.

Figure 8 shows discharge capacity versus cycle number of lithium powder polymer batteries assembled with composite gel polymer electrolytes containing different amounts of

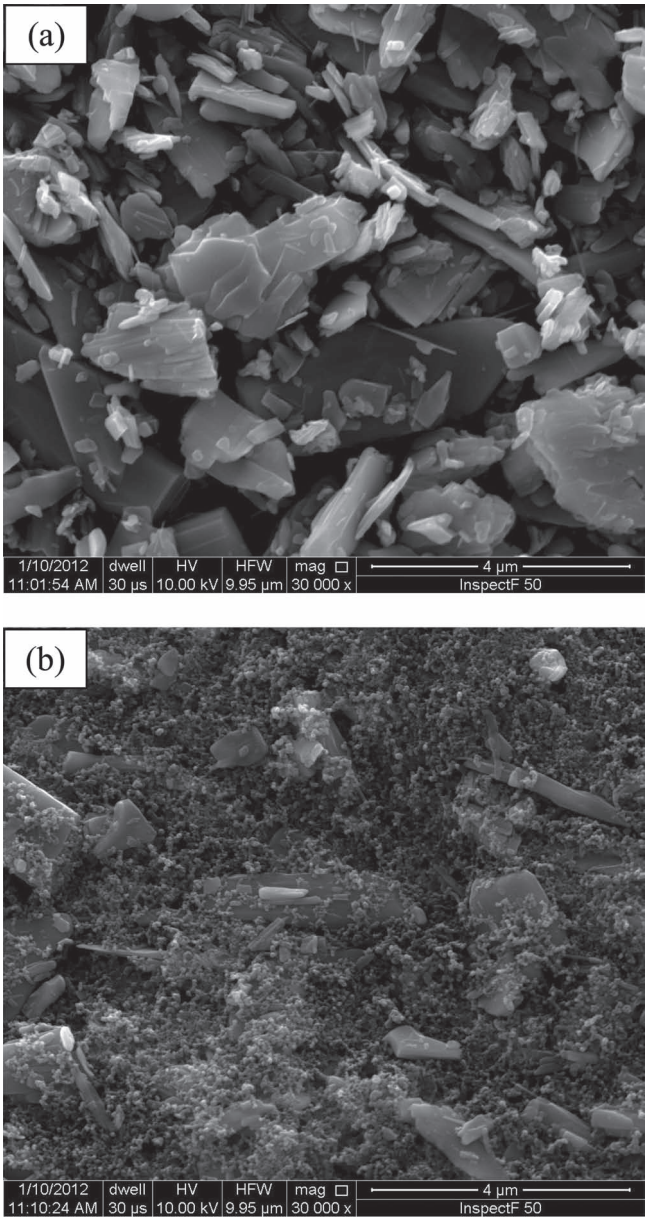

Figure 6. SEM images of (a) the LiV_3O_8 powders, and (b) the cathode prepared with LiV_3O_8 powders.

$SiO_2(Li^+)$ particles. For the purpose of comparison, the cycling result of the cell assembled with liquid electrolyte is also given in the figure. The initial discharge capacity slightly increased with the addition of $SiO_2(Li^+)$ up to 20 wt.% in accordance with the associated increase in ionic conductivity. The capacity retention was also improved by adding the $SiO_2(Li^+)$ particles into the gel polymer electrolyte. As discussed earlier, the hydrophilic PLS in the shells of the $SiO_2(Li^+)$ particles holds the solvent more effectively, and the ability to retain the electrolyte solution in the composite gel polymer electrolyte is favored by the addition of $SiO_2(Li^+)$ powder, which helps to prevent the release of the electrolyte solution that is highly reactive toward lithium metal. The enhancement of interfacial stability promoted by

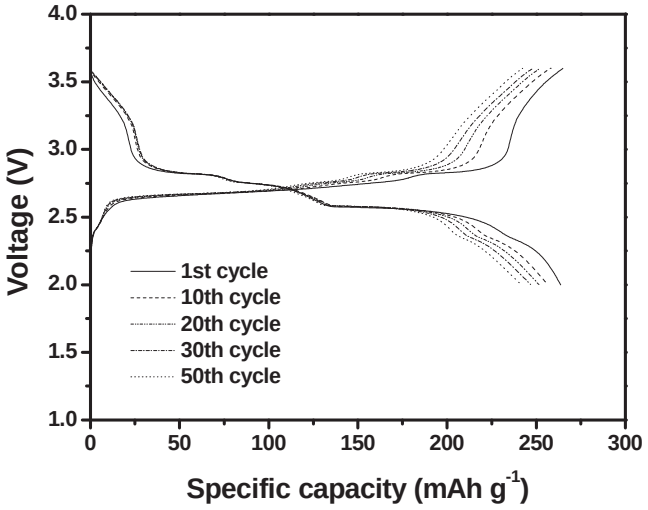

Figure 7. Charge and discharge curves of the lithium powder polymer battery (Li/LiV_3O_8) assembled with the composite gel polymer electrolyte containing 20 wt.% $SiO_2(Li^+)$ particles (0.2 C rate, cut-off: 2.0–3.6 V).

the $SiO_2(Li^+)$ nanoparticle may also have contributed to the improved capacity retention, as reported for other composite polymer electrolyte systems using plain inorganic materials such as SiO_2, Al_2O_3, TiO_2 and $BaTiO_3$.[25,49,50] It should be noted that the batteries with the composite gel polymer electrolytes containing $SiO_2(Li^+)$ powders exhibited higher initial discharge capacity and better capacity retention than the battery assembled with liquid electrolyte. The ionic conductivity of the liquid electrolyte used in this study is 7.1×10^{-3} S cm^{-1}. However, the ionic conductivity (1.3×10^{-4} S cm^{-1}) of the polypropylene separator filled with the electrolyte solution in the cell is much lower than that of the electrolyte solution, as the specific resistivity of the separator saturated with liquid electrolyte is increased by the combination of tortuosity and porosity of the separator.[51]

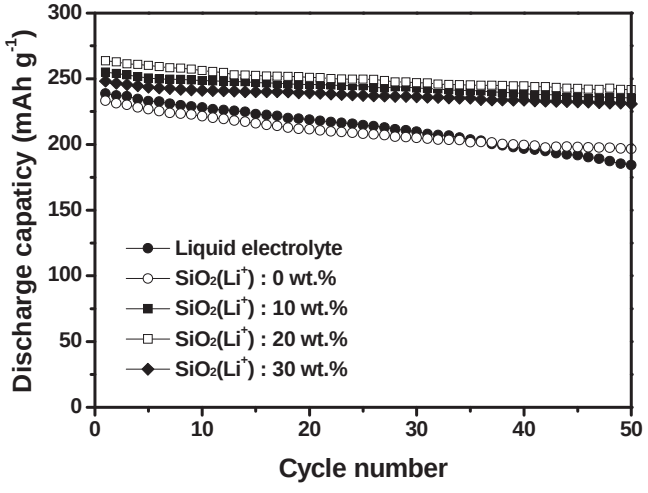

Figure 8. Discharge capacities of the lithium powder polymer batteries (Li/LiV_3O_8) assembled with the composite gel polymer electrolyte containing different contents of $SiO_2(Li^+)$ particles (0.2 C rate, cut-off: 2.0–3.6 V, 25 °C).

Thus, the ionic resistance is higher in the liquid electrolyte-based cell than in the cells assembled with composite gel polymer electrolytes, which gives rise to the reduction of initial discharge capacity. The capacity decline of the lithium powder battery with liquid electrolyte may indicate the gradual formation and growth of lithium dendrites during charge-discharge cycles. These dendrites lower the cycling efficiency and cause a decline of reversible capacity with cycling.

SEM analysis of the lithium powder electrodes was performed after charge-discharge cycles to investigate the cause of the improved capacity retention in the batteries assembled with composite gel polymer electrolytes. **Figure 9** shows the SEM

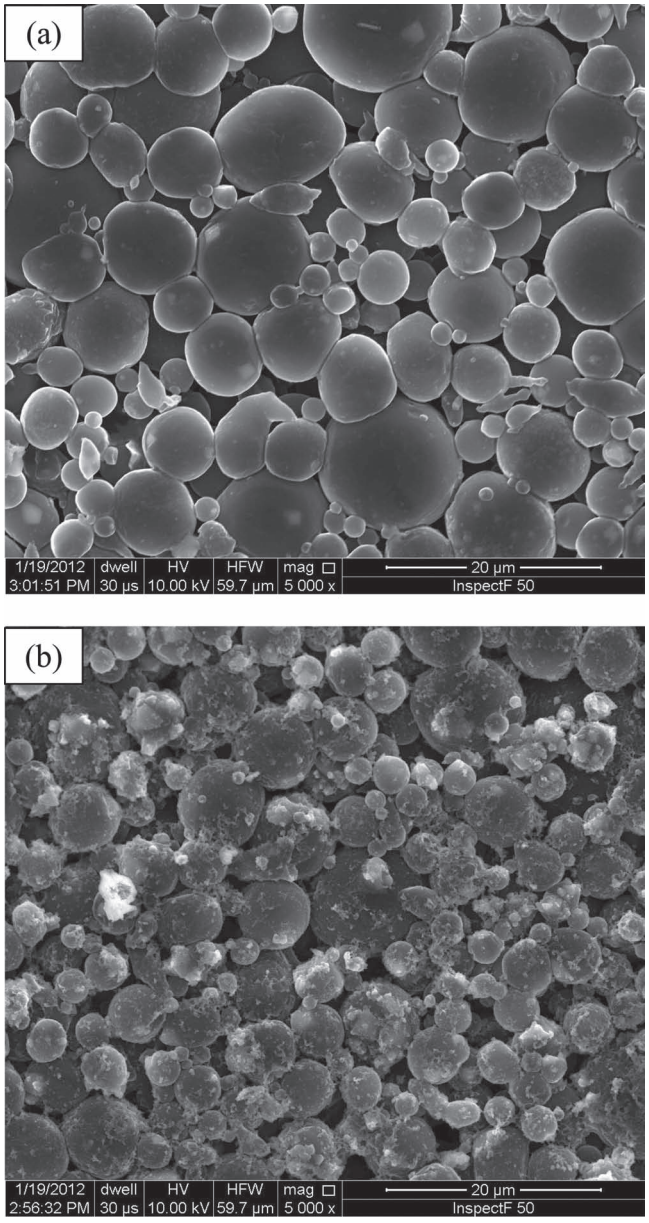

Figure 9. SEM images on the surface of the lithium powder electrodes cycled in (a) composite gel polymer electrolyte and (b) liquid electrolyte, which are obtained after 50 cycles.

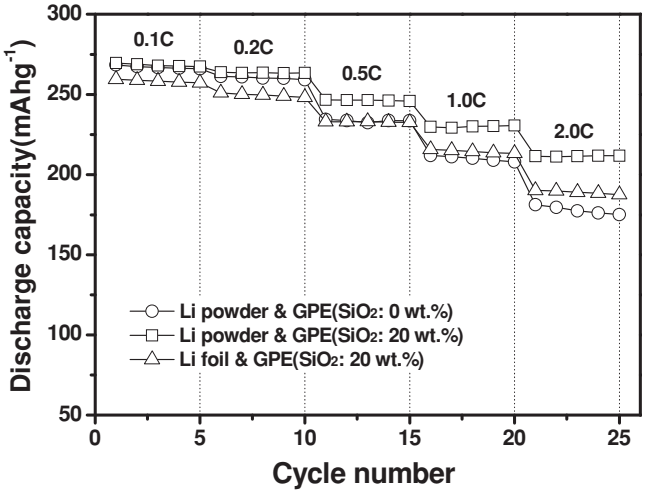

Figure 10. Cycling performance of lithium metal polymer batteries assembled with different anodes and electrolytes. The C-rate was increased from 0.1 to 2.0 C after every 5 cycles. GPE means a gel polymer electrolyte.

images of the surface of lithium powder electrodes after 50 cycles. Before cycling, the average diameter of original lithium powder was about 7 μm. After cycling of cell assembled with the composite gel polymer electrolyte, no dendrites formed on the lithium powder surface, and the individual lithium powders retained most of their original spherical shapes. That is to say, there was little change in electrode morphology after cycling. On the other hand, in the case of lithium powder electrode cycled in the liquid electrolyte, though most of the powders seemed spherical, some dirt or scattered pits were observed on the lithium powder surface, which might grow to dendrite for further cycling. These results suggest that the use of composite gel polymer electrolyte without continuous free electrolyte solution paths for lithium dendrites to propagate may effectively suppress the dendrite growth during cycling. Accordingly, lithium powder batteries assembled with composite polymer electrolytes exhibited stable cycling characteristics compared to that of the lithium powder battery with liquid electrolyte.

Figure 10 compares the discharge capacities of the lithium power batteries assembled with different electrolytes, with the C-rate increasing from 0.1 to 2.0 C every five cycles. Cycling results of lithium polymer battery assembled with lithium foil anode and composite gel polymer electrolyte containing 20 wt.% $SiO_2(Li^+)$ particles are also shown for comparison in the figure. It is notable that the discharge capacities of the lithium powder polymer battery are higher than those of the lithium foil polymer battery at all C-rates tested. Because the surface area of the lithium powder electrode for charge transfer reaction ($Li \leftrightarrow Li^+ + e$) is larger than that of the lithium foil electrode, the two electrodes may experience different effective current densities even though the batteries are cycled at the same current density. As a result, the lithium powder polymer battery exhibits higher discharge capacities than the lithium foil polymer battery, and the difference in discharge capacities between two battery systems increases with increasing C-rate. It is also found that both the discharge capacity and capacity retention of the lithium powder batteries are improved by adding core-shell structured $SiO_2(Li^+)$ particles into the gel polymer electrolyte. As discussed with data in Figure 5, both ionic conductivity and lithium transport number increase with the addition of $SiO_2(Li^+)$ particles, which reduces the concentration polarization of the electrolyte during cycling and provides higher discharge capacity at high current rates. The favorable interfacial characteristics promoted by the $SiO_2(Li^+)$ powder also lead to the improved capacity retention through cycling. Our results suggest that the composite gel polymer electrolytes prepared with core-shell structured $SiO_2(Li^+)$ particles are promising electrolyte materials for use in lithium metal polymer batteries with high energy density and good capacity retention. It encourages us to continue the study on advanced lithium batteries, such as lithium-air or lithium-sulfur, with the aim of achieving high cycling performance by applying the composite gel polymer electrolytes containing core-shell structured $SiO_2(Li^+)$ particles as electrolyte materials.

3. Conclusions

Core-shell structured SiO_2 nanoparticles were synthesized by radical polymerization of 4-styrenesulfonic acid sodium salt with spherical SiO_2 core materials containing vinyl groups. The composite gel polymer electrolytes prepared with core-shell structured $SiO_2(Li^+)$ particles exhibited high ionic conductivity and sufficient mechanical properties for use in rechargeable lithium batteries. The lithium powder polymer batteries assembled with lithium powder anode, composite gel polymer electrolyte and LiV_3O_8 cathode delivered a high initial discharge capacity and exhibited stable cycling characteristics. The morphological analysis of the lithium powder electrode demonstrated that the dendritic growth of lithium could be effectively suppressed by using composite gel polymer electrolytes. It is expected that the advanced lithium metal polymer batteries with high energy density and good capacity retention can be produced by careful selection of cathodes with high specific capacity.

4. Experimental Section

Synthesis of core-shell structured silica particles: The core-shell structured $SiO_2(Li^+)$ particles were synthesized through three steps (Figure S1), as reported earlier.[52] Different amounts of VTMS were added to double distilled water (150 mL) under stirring for 30 minutes until the oil (VTMS) droplets completely disappeared and a transparent solution was obtained. NH_4OH (0.1 mL) was then added to the solution and the reaction (hydrolysis and condensation) was continued for 12 h at room temperature. After completion of the reaction, the resulting precipitate was centrifuged and washed several times with ethanol. Silica core materials of different sizes were obtained. Core-shell $SiO_2(Na^+)$ particles were synthesized by radical copolymerization of cored-silica particles with 4-styrenesulfonic acid sodium salt, as reported in similar systems.[44,53] The silica core particles (1.5 g) were dispersed in n-methyl pyrrolidone (NMP) via ultrasonication for 30 min, and a solution consisting of 4-styrenesulfonic acid sodium salt (6.0 g) and azobisisobutyronitrile (AIBN, 0.4 g) dissolved in NMP was added. To induce polymerization, the mixture was heated to 60 °C with stirring for 72 h. After polymerization, the solution was precipitated into excess diethyl ether with vigorous stirring. The precipitate was filtered and

washed with methanol/ethanol several times. The Na^+ ions in the core-shell structured $SiO_2(Na^+)$ particles were replaced by Li^+ ions by ionic exchange with $LiOH{\cdot}H_2O$.[54] The resulting core-shell $SiO_2(Li^+)$ powders were washed with ethanol to remove any impurities and dried under vacuum at 110 °C for 12 h.

Preparation of composite gel polymer electrolytes: A hybrid composite polymer membrane consisting of P(VdF-*co*-HFP) and core-shell structured $SiO_2(Li^+)$ powders was prepared as follows. P(VdF-*co*-HFP), $SiO_2(Li^+)$ powders and dibutyl phthalate (DBP) were mixed in acetone using ball milling for 12 hr, and cast to a thickness of 500 μm using a doctor blade. After 30 min, the cast film was immersed in methanol to remove DBP. The resulting membrane was vacuum dried at 70 °C for at least 12 h. The content of $SiO_2(Li^+)$ powder in the prepared composite polymer membranes varied from 0 to 30 wt.%. Free-standing composite gel polymer electrolyte films were finally obtained by soaking the composite polymer membranes in a 1.15 M $LiPF_6$-ethylene carbonate (EC)/diethyl carbonate (DEC) (3:7 by volume, battery grade, Techno Semichem Co.) solution. The uptake of the liquid electrolyte solution was determined by the equation:

$$\text{Uptake}(\%) = \left(W_g - W_m\right)/W_m \times 100, \quad (1)$$

where W_g and W_m are the weights of the gel polymer electrolyte and dry membrane, respectively.

Electrode preparation and cell assembly: Lithium powders were prepared by the droplet emulsion technique (DET),[5,8] and Figure S6 shows the schematic diagram of the DET apparatus. A mixture of molten lithium and carrier fluid (silicone oil) was sheared at approximately 25,000 rpm to produce an emulsion. As the emulsion was cooled to room temperature, the liquid lithium droplets solidified to form powders. These lithium powders were separated from the silicone oil and cleaned with hexane. To make them into the form of an electrode, the lithium powders were compacted by pressing at 15 MPa. The thickness of the lithium powder electrode was about 40 μm. The LiV_3O_8 cathode was prepared by coating a slurry containing 80 wt.% lithium vanadate (GfE, Germany), 15 wt.% Ketchen black and 5 wt.% CMC on an Al foil. The electrode was roll pressed to enhance particulate contact and adhesion to the current collector. The thicknesses of the electrodes ranged from 25 to 30 μm after roll pressing. Lithium powder polymer batteries were assembled by sandwiching the composite gel polymer electrolyte between the lithium powder anode and the LiV_3O_8 cathode. For comparison, a liquid electrolyte-based lithium powder battery was also assembled with a polypropylene separator (Celgard 2400) and liquid electrolyte (1.15 M $LiPF_6$-EC/DEC) instead of a composite gel polymer electrolyte. The cells were enclosed in a metallized plastic bag and vacuum-sealed. All the batteries were assembled in a dry box filled with argon gas.

Measurements: The morphologies of the materials were examined using a scanning electron microscope (SEM, JEOL JSM-6300) and a transmission electron microscope (TEM, JEOL 2010). Fourier transform infrared (FT-IR) spectra were recorded on a Magna IR 760 spectrometer in the range of 400-4000 cm^{-1} with KBr powder-pressed pellets. The elemental composition of the core-shell structured SiO_2 particles was determined using energy dispersive X-ray spectroscopy (EDXS). X-ray photoelectron spectra (XPS) measurements of the $SiO_2(Li^+)$ powders were performed on an ESCALAB Mark ‖ with an Al Kα(X-ray) lamp. The lithium transport number was measured by a combination of AC impedance and DC polarization methods.[55] AC impedance measurements were performed to measure ionic conductivity and interfacial resistance using an impedance analyzer over a frequency range of 1 mHz to 100 kHz with an amplitude of 10 mV. Charge and discharge cycling tests of the lithium powder polymer batteries were conducted over a voltage range of 2.0–3.6 V with battery test equipment at room temperature. To observe the morphological changes of the lithium powder electrodes, the cells were disassembled after 50 cycles in a dry room and the electrodes were washed with dimethyl carbonate to remove the residual electrolyte. After drying in an argon-filled glove box, the morphology of the lithium powder electrodes was characterized using a field emission scanning electron microscope.

Supporting Information

Supporting Information is available from the Wiley Online Library or from the author.

Acknowledgements

This work was supported by Pohang Steel Corporation (POSCO) and Research Institute of Industrial Science & Technology (RIST, No. 2011K128). This work was also partially supported by a grant from the Fundamental R&D Program for Core Technology of Materials and the Energy Efficiency & Resources of the Korea Institute of Energy Technology Evaluation and Planning (20112010100110) grant, and a National Research Foundation of Korea (NRF) grant funded by the Korean government (MEST, 2011-0028757).

Received: March 13, 2012
Revised: April 10, 2012
Published online: May 21, 2012

[1] J.-M. Tarascon, M. Armand, *Nature* **2001**, *414*, 359.
[2] M. Mori, Y. Naruoka, K. Naoi, D. Fauteux, *J. Electrochem. Soc.* **1998**, *145*, 2340.
[3] D. Aurbach, E. Zinigard, Y. Cohen, H. Teller, *Solid State Ionics* **2002**, *148*, 405.
[4] I. W. Seong, C. H. Hong, B. K. Kim, W. Y. Yoon, *J. Power Sources* **2008**,*178*, 769.
[5] W. Y. Yoon, J. S. Paik, D. Lacourt, J. H. Perepezko, *J. Appl. Phys.* **1986**, *60*, 3489.
[6] S. T. Hong, J. S. Kim, S. J. Lim, W. Y. Yoon, *Electrochem. Acta* **2004**, *50*, 535.
[7] J. H. Chung, W. S. Kim, W. Y. Yoon, S. W. Min, B. W. Cho, *J. Power Sources* **2006**, *163*, 191.
[8] J. S. Kim, S. H. Baek, W. Y. Yoon, *J. Electrochem. Soc.* **2010**, *157*, A984.
[9] M. B. Armand, T. M. Chabagno, M. Duclot, in *Proceedings of the Second International Meeting on Solid Electrolytes*, St. Andrews, Scotland, September **1978** (Extended Abstract).
[10] M. B. Armand, *Solid State Ionics* **1994**, *69*, 309.
[11] W. H. Meyer, *Adv. Mater.* **1998**, *10*, 439.
[12] A. S. Arico, P. Bruce, B. Scrosati, J.-M. Tarascon, W. Van Schalkwijk, *Nat. Mater* **2005**, *4*, 366.
[13] L.-Z Fan, Y.-S. Hu, A. J. Bhattacharyya, J. Maier, *Adv. Funct. Mater.* **2007**, *17*, 2800.
[14] J. Y. Song, Y. Y. Wang, C. C. Wan, *J. Power Sources* **1999**, *77*, 183.
[15] J. W. Fergus, *J. Power Sources* **2010**, *195*, 4554.
[16] G. B. Appetecchi, F. Croce, B. Scrosati, *Electrochim. Acta* **1995**, *40*, 991.
[17] D. Peramunage, D. M. Pasquariello, K. M. Abraham, *J. Electrochem. Soc.* **1995**, *42*, 1789.
[18] J. M. Tarascon, A. S. Gozdz, C. N. Schmutz, F. Shokoohi, P. C. Warren, *Solid State Ionics* **1996**, *49*, 86.
[19] D. W. Kim, K. A. Noh, H. S. Min, D. W. Kang, Y. K. Sun, *Electrochem. Solid State Lett.* **2002**, *5*, A63.
[20] S. W. Choi, J. R. Kim, Y. R. Ahn, S. M. Jo, E. J. Cairns, *Chem. Mater.* **2007**, *19*, 104.
[21] M. C. Borghini, M. Mastragostino, S. Passerini, B. Scrosati, *J. Electrochem. Soc.* **1995**, *142*, 2118.

[22] J. Fan, P. S. Fedkiw, *J. Electrochem. Soc.* **1997**, *144*, 399.
[23] D. W. Kim, Y. K. Sun, *J. Electrochem. Soc.* **1998**, *145*, 1958.
[24] D. E. Strauss, D. Golodnitsky, E. Peled, *Electrochem. Solid State Lett.* **1999**, *2*, 115.
[25] F. Croce, G. B. Appetecchi, L. Persi, B. Scrosati, *Nature* **1998**, *394*, 456.
[26] H. Han, W. Liu, J. Zhang, X.-Z. Zhao, *Adv. Funct. Mater.* **2005**, *15*, 1940.
[27] A. M. Stephan, K. S. Nahm, *Polymer* **2006**, *47*, 5952.
[28] C. M. Yang, H. S. Kim, B. K. Na, K. S. Kum, B. W. Cho, *J. Power Sources* **2006**, *156*, 574.
[29] J. Syzdek, M. Armand, M. Marcinek, A. Zalewska, G. Zukowska, W. Wieczorek, *Electrochim. Acta* **2010**, *55*, 1314.
[30] S. K. Das, S. S. Mandal, A. J. Bhattacharyya, *Energy Environ.Sci.* **2011**, *4*, 1391.
[31] N. S. Choi, Y. M. Lee, B. H. Lee, J. A. Lee, J. K. Park, *Solid State Ionics* **2004**, *167*, 293.
[32] J. Sun, P. Bayley, D. R. MacFarlane, M. Forsyth, *Electrochim. Acta* **2007**, *52*, 7083.
[33] J. Nordstrom, A. Matic, J. Sun, M. Forsyth, D. R. MacFarlane, *Soft Matter* **2010**, *6*, 2293.
[34] K. Nassau, D. W. Murphy, *J. Non-Cryst. Solids* **1981**, *44*, 297.
[35] S. Panero, M. Pasquali, G. Pistoia, *J. Electrochem. Soc.* **1983**, *130*, 1225.
[36] K. West, Z. Bachau-C, S. Skaarup, Y. Saidi, J. Barker, I. I. Olsen, R. Pynenburg, R. Koksbang, *J. Electrochem. Soc.* **1996**, *143*, 820.
[37] S. Jouanneau, A. L. La Salle, A. Verbaere, D. Guyomard, *J. Electrochem. Soc.* **2005**, *152*, A1660.
[38] N. Tran, K. G. Bramnik, H. Hibst, J. Prolb, N. Mronga, M. Holzapfel, W. Scheifele, P. Novak, *J. Electrochem. Soc.* **2008**, *155*, A384.
[39] H. Liu, Y. Wang, W. Yang, H. Zhou, *Electrochim. Acta* **2011**, *56*, 1392.
[40] Y. Q. Qiao, X. L. Wang, J. P. Zhou, J. Zhang, C. D. Gu, J. P. Tu, *J. Power Sources* **2012**, *198*, 287.
[41] J. P. Blitz, R. S. S. Murthy, D. E. Leyden, *J. Colloid Interface Sci.* **1988**, *121*, 63.
[42] P. Siberzan, L. Leger, D. Ausserre, J. J. Benatta, *Langmuir* **1991**, *7*, 1647.
[43] C. P. Tripp, M. L. Hair, *Langmuir* **1992**, *8*, 1120.
[44] V. Nguyen, W. Yoshida, Y. Cohen, *J. Appl. Polymer. Sci.* **2002**, *87*, 300.
[45] S. H. Goh, S. Y. Lee, X. Luo, C. H. A. Huan, *Polymer* **2000**, *41*, 211.
[46] M. S. Kang, J. H. Kim, J. Won, Y. S. Kang, *J. Phys. Chem. C* **2007**, *111*, 5222.
[47] H. E. Park, I. W. Seong, W. Y. Yoon, *J. Power Sources* **2009**, *189*, 499.
[48] J. Kawakita, T. Miura, T. Kishi, *J. Power Sources* **1999**, *83*, 79.
[49] F. Croce, B. Scrosati, *J. Power Sources* **1993**, *43*, 9.
[50] M. C. Borghini, M. Mastragostino, S. Passerini, B. Scrosati, *J. Electrochem. Soc.* **1995**, *142*, 2118.
[51] P. Arora, Z. Zhang, *Chem. Rev.* **2004**, *104*, 4419.
[52] Y. S. Lee, S. H. Ju, J. H. Kim, S. S. Hwang, J. M. Choi, Y. K. Sun, H. Kim, B. Scrosati, D. W. Kim, *Electrochem. Commun.* **2012**, *17*, 18.
[53] G Liu, H. Zhang, X. Yang, Y. Wang, *Polymer* **2007**, *48*, 5896.
[54] C. H. Park, Y. K. Sun, D. W. Kim, *Solid State Ionics* **2004**, *50*, 375.
[55] J. Evance, C. A. Vincent, P. G. Bruce, *Polymer* **1987**, *28*, 2324.